Seasonal Variations in Flocculation and Erosion Affecting the Large-Scale Suspended Sediment Distribution in the Scheldt Estuary
The Importance of Biotic Effects

Horemans, Dante M.L.; Dijkstra, Yoeri M.; Schuttelaars, Henk M.; Sabbe, Koen; Vyverman, Wim; Meire, Patrick; Cox, Tom J.S.

Citation (APA)
Horemans, D. M. L., Dijkstra, Y. M., Schuttelaars, H. M., Sabbe, K., Vyverman, W., Meire, P., & Cox, T. J. S. (2021). Seasonal Variations in Flocculation and Erosion Affecting the Large-Scale Suspended Sediment Distribution in the Scheldt Estuary: The Importance of Biotic Effects. *Journal of Geophysical Research: Oceans*, *126*(4), Article e2020JC016805. https://doi.org/10.1029/2020JC016805

Important note
To cite this publication, please use the final published version (if applicable).
Please check the document version above.

Seasonal Variations in Flocculation and Erosion Affecting the Large-Scale Suspended Sediment Distribution in the Scheldt Estuary: The Importance of Biotic Effects

Dante M. L. Horemans[1] [ID], **Yoeri M. Dijkstra[2]** [ID], **Henk M. Schuttelaars[2]** [ID], **Koen Sabbe[3]** [ID], **Wim Vyverman[3]** [ID], **Patrick Meire[1]** [ID], and **Tom J. S. Cox[1,4]** [ID]

[1]Ecosystem Management Research Group, University of Antwerp, Wilrijk, Belgium, [2]Delft Institute of Applied Mathematics, Delft University of Technology, Delft, the Netherlands, [3]Protistology and Aquatic Ecology Lab, Ghent University, Ghent, Belgium, [4]NIOZ Royal Netherlands Institute for Sea Research, Yerseke, the Netherlands

Abstract Many estuaries exhibit seasonality in the estuary-scale distribution of suspended particulate matter (SPM). This SPM distribution depends on various factors, including freshwater discharge, salinity intrusion, erodibility, and the ability of cohesive SPM to flocculate into larger aggregates. Various authors indicate that biotic factors, such as the presence of algae and their excretion of sticky transparent exopolymer particles (TEP), affect the flocculation and erosion processes. Consequently, seasonality in these biotic factors may play a role in the observed seasonality in SPM. Whereas the impact of abiotic factors on seasonality in SPM is well studied, the relative contribution of biotically induced seasonality is largely unknown. In this study, we employ two approaches to assess the aggregated importance of biotically induced seasonality in flocculation and erosion on seasonality in SPM in the Scheldt estuary. In the first approach, we focus on seasonality of in situ observations in the Scheldt estuary of turbidity, floc size, Chlorophyll-a, and TEP, showing that the abiotic parameters show seasonality, while seasonality in TEP is ambiguous. The second approach concerns a reverse engineering method to calibrate biotically affected parameters of a coupled sediment transport-flocculation model to turbidity observations, allowing us to compare the modeled SPM concentrations to the observations. Driven by seasonality in freshwater discharge, the model captures the observed seasonality in SPM without requiring biotically induced seasonality in flocculation and erosion, which is supported by the absence of seasonality in TEP.

Plain Language Summary Estuaries often show regions in which the water is more turbid due to a local elevation of suspended sediment. This local elevation regularly displays seasonality, which is partially driven by seasonality in the erosion properties of the sediment bed and the ability of suspended sediment to flocculate into larger flocs. Two crucial factors impacting the erosion and flocculation processes are the presence of algae and the corresponding excreted sticky substances, which are reported to stabilize the sediment bed but can also glue the suspended sediment particles together. In the present study, we study the aggregated importance of such biotic factors to seasonality in suspended sediment concentrations, applied to the Scheldt estuary. We first focus on seasonality of field observations of suspended sediment concentration, floc size, algal abundance, and the sticky substances excreted by the algae, all showing seasonality except the sticky substances. Next, we use a model that simulates the erosion, flocculation, and accumulation of suspended sediment to quantify a potential seasonality in the impact of biotic factors on flocculation and erosion. Surprisingly, we do not require seasonality in the impact of biotic factors on flocculation and erosion to explain the observed seasonality in sediment dynamics, which is supported by the absence of seasonality in the sticky substances excreted by the algae.

1. Introduction

The suspended particulate matter (SPM) concentrations in estuaries often show regions in which SPM accumulates, resulting in zones with locally elevated SPM concentrations. These regions are called estuarine turbidity maxima (ETM), of which both the magnitude and location can show a significant seasonality. Such seasonality was observed in, for example, the Scheldt estuary (Cox et al., 2019), the Chesapeake Bay (Stanford et al., 2001), the Weser (Kappenberg & Grabemann, 2001), and the Hudson River estuary (Ralston et al., 2012). This seasonality in ETM is driven by seasonality in factors affecting transport of SPM, such as

freshwater discharge (Allen et al., 1980; Uncles et al., 2006), salinity (MacCready & Geyer, 2010), erosion properties of the sediment bed (Stal, 2010), and settling velocity (Fettweis et al., 2014; Kranenburg, 1994; Verney et al., 2009; Winterwerp & van Kesteren, 2004). The latter two are related to both abiotic seasonal variations, such as variations in turbulence, salinity, and SPM (Dyer, 1989; Lai et al., 2018; van Leussen, 1994) and biotic variations (Alldredge et al., 1993; Frostick & McCave, 1979; Passow et al., 2001).

Biotic seasonality may impact the erosion properties of the sediment bed in multiple ways. On the one hand, various authors found that algal activity, which typically peaks in spring and summer, often stabilizes the sediment bed (Frostick & McCave, 1979) and induces the formation of bedforms (Malarkey et al., 2015) by, for example, the excretion of extracellular polymeric substances (EPS), of which sticky transparent exopolymer particles (TEP) are a particulate form (Passow, 2002), and which bind the sediment together (Stal, 2010). On the other hand, the subsequent grazing of the algae by bioturbatory macroheterotrophs may generate an increase in erodibility (Paterson & Black, 1999).

Beside erosion properties of the sediment bed, biotic factors may also impact flocculation, which is defined as the aggregation and break-up of cohesive SPM, resulting in seasonal variations of the settling velocity of SPM flocs. Biotic characteristics, such as organic content, directly influence the differential density and structure of flocs (Fall et al., 2021; Kranenburg, 1994; van Leussen, 1994). Furthermore, organic content impacts, for example, the floc strength and collision efficiency (Winterwerp & van Kesteren, 2004), averaged floc size (Mietta et al., 2009), and floc break-up (Alldredge et al., 1990). Finally, in situ observations show a correlation between Chlorophyll-a (Chl-a) and flocculation efficiency (Verney et al., 2009), and TEP and floc strength (Fettweis et al., 2014).

These biotic seasonal variations in the settling velocity and erosion properties of the sediment bed are hypothesized to affect seasonality in ETM characteristics in estuaries. However, this hypothesis has not been systematically investigated. Therefore, in this contribution, we focus on quantifying the importance of such biotic seasonal variations to the seasonality in ETM, applied to the Scheldt estuary (Belgium and the Netherlands).

The Scheldt estuary is a particularly good example to study the influence of biotic seasonal variations on the seasonality in ETM for two reasons. First, the settling velocity and erosion properties have been found to be important to the ETM formation (Brouwer et al., 2018; Horemans et al., 2020) and the corresponding floc size dynamics have been related to biotic activity (M. S. Chen et al., 2005; P. H. Chen et al., 2018; Wartel & Francken, 1998). Second, a recent study by Cox et al. (2019) reported a change in the seasonal ETM patterns and suggested that a change in biotically induced flocculation dynamics may be responsible for this change.

Assessing the relative importance of the abiotic and biotic factors that impact seasonality in SPM is challenging because of their strong interdependence. In addition, while reasonably accurate models exist to parameterize the effect of abiotic flocculation and erosion, explicit parameterizations of biotic effects relating, for example, Chl-a and TEP to flocculation and erodibility, rely on many assumptions (see Lai et al., 2018 for a recent review). This makes it difficult to dynamically solve the impact of biota on the large-scale ETM dynamics through flocculation and erosion, using explicitly defined bio-physical-chemical interactions.

In view of this, we employ a reverse engineering approach, combined with a detailed analysis of observations to assess the influence of biotically induced seasonality in flocculation and erosion on the large-scale SPM dynamics. Concerning the observations, we quantitatively study the seasonality in observed turbidity (cf. SPM), floc size, Chl-a, and TEP. This provides information on the seasonality of SPM dynamics, flocculation, and biota. Taking a reverse engineering model approach, following P. H. Chen et al. (2018), the model does not rely on explicit model parameterizations for biotic flocculation and erosion. Instead, the accumulated biotic impact is accounted parametrically, using two empirical parameters; one in the flocculation model of Horemans et al. (2020) and one in the erosion model (Dijkstra et al., 2019; Kandiah, 1974; Partheniades, 1965). Abiotic seasonal variations, including variations of the river discharge, salinity, and abiotic effects on flocculation and erosion are explicitly taken into account. The two biotically affected parameters are calibrated to long-term SPM observations of both summer and winter conditions in the Scheldt estuary. We hypothesize that, if a seasonality in biological factors were to have a significant impact on the large-scale SPM distribution, we would obtain a significantly different value of these biotically affected parameters to represent summer and winter conditions in the Scheldt estuary.
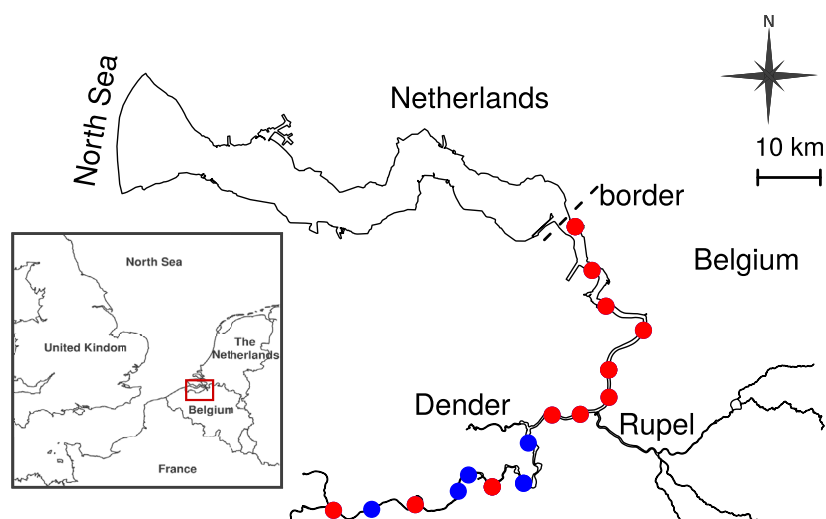
Figure 1. The Scheldt estuary and its two main tributaries (Rupel and Dender). The dots represent the locations where monthly and biweekly turbidity and floc size profiles were measured in the frame of the OMES (Dutch: "Onderzoek Milieu Effecten Sigmaplan") environmental monitoring program. The transparent exopolymer particles (TEP) concentration was only measured at 11 instead of the 16 stations, depicted in red.

2. Material and Methods

In this section, we first discuss some of the characteristics of the Scheldt estuary. Next, the measurement methods used to obtain the in situ observations are introduced and the model approach is presented.

2.1. Study Area

The Scheldt estuary is ∼160 km long, funnel-shaped estuary (see Figure 1). It flows through Belgium into the North Sea near Vlissingen (the Netherlands). Because of its relatively small freshwater discharge, the Scheldt estuary can be considered a tide-dominated and well-mixed estuary (Meire et al., 2005). The total time-averaged freshwater discharge Q over the years 2015–2018 equals 40 m^3 s^{-1} and 174 m^3 s^{-1} in summer (June–August) and winter (January–March), respectively (Waterinfo.be, 2019). The main tributaries of the Scheldt estuary are the Rupel and the Dender. The Upper Sea Scheldt boundary (i.e., the upstream boundary of the Scheldt estuary), the Rupel, and the Dender are responsible for 16.4%, 77.2%, and 6.4% of the total river discharge in summer and 35.4%, 53.1%, and 11.5% in winter, respectively.

The maintenance of the navigation channel to the port of Antwerp (first four red dots from the Dutch-Belgian border in Figure 1) requires intensive dredging activities. To minimize the risk of flooding, the dredged material is dumped back into the Scheldt estuary, which comes with significantly higher SPM loads (10^6 ton year^{-1}) than the fluvial input (Dijkstra et al., 2019). At the main dumping locations at 73 and 78 km from the mouth, the time-averaged dumped material between 2001 and 2015 corresponds to high SPM input of ∼60 and 100 kg s^{-1}, respectively. Consequently, these dumping activities impact the SPM concentration locally, which was confirmed by a multivariate regression analysis of SPM observations between 1996 and 2016. This analysis showed that the SPM concentrations at the dumping sites are dominantly correlated to dumping activities (IMDC, 2016). The yearly fluvial input of SPM at the upstream boundary and tributaries is of the order of 10^4–10^5 ton year^{-1} and is assumed to scale linearly with the freshwater discharge (Dijkstra et al., 2019; Plancke et al., 2017).

2.2. In Situ Observations

The Belgian part of the Scheldt estuary has been monitored by the long-term OMES (Dutch: "Onderzoek Milieu Effecten Sigmaplan") monitoring campaign (Maris & Meire, 2017). Within this campaign, various variables, including turbidity, SPM, salinity, primary particle size, floc size, Chl-a, and TEP concentration,

have been measured biweekly or monthly and independently of the tidal phase and spring-neap tide at 16 fixed stations (see Figure 1). In the following, we discuss the measurement methods to obtain the observations of the four variables we focus on: turbidity (Maris et al., 2021b), floc size (Maris et al., 2021a), Chl-a (Maris & Meire, 2021), and TEP (Vyverman et al., 2021).

Turbidity depth-profiles were measured over the years 2015–2018 using an Optical Backscatter point Sensor (OBS) of RBR type XR420 CTD+. To translate turbidity to SPM concentration, we simultaneously collected two SPM samples at approximately the water surface and half the water depth and applied a linear data fit (Horemans et al., 2020). The observations cover 18 and 14 campaigns in summer (June–August) and winter (January–March), respectively, resulting in 18 and 14 SPM profiles at each of the 16 locations.

From September 2017 until January 2019, floc size profiles were measured mainly in the upper half of the water column, simultaneously with the turbidity profiles. Floc size was measured using an optical laser diffraction instrument, a Sequoia Laser In Situ Scattering and Transmissometry (LISST) 200x instrument. The LISST 200x instrument measures the floc size volume distribution for 36, nonequidistant size classes with a floc size ranging between 1 and 500 µm. This particle size distribution was used to determine the geometric averaged floc size following the averaging-method of Sequoia Scientific (2019) to correct for the nonequidistant size classes. Because the estimated floc size is highly sensitive to the averaging method, we also use two additional averaging methods in Appendix A.

Simultaneously with the turbidity and floc size profiles, bucket samples at the water surface were taken to estimate the Chl-a and TEP concentration. The TEP measurements only started in 2018. We estimated the Chl-a concentration, following the spectrophotometric method described in Rice et al. (2017) that corrects for turbidity, chlorophyll b, chlorophyll c, and pheophytin pigments. We used 50 ml water samples, a 1 cm pathway cuvette, and a Shimadzu UV-1700 spectrophotometer. The detection threshold of the method is $\sim 10~\mu g~l^{-1}$. When Chl-a values are below this threshold value, they are put to $10~\mu g~l^{-1}$. The total number of observed Chl-a concentrations per stations equals 24 in summer and ranges from 11 upto 13 in winter, depending on the station. TEP concentrations were estimated according to the colorimetric method described in Claquin et al. (2008), adapted from the original method described in Passow and Alldredge (1995). TEP concentrations were only measured once a month at 11 stations (see Figure 1, red dots), resulting in 66 estimates in both summer and winter.

2.3. Model and Model Experiments

iFlow model: The model used is the process-based, width-averaged, idealized model called iFlow that solves for water motion and SPM trapping in tide-dominated estuaries using the width-averaged shallow water and SPM mass balance equations in equilibrium condition (Dijkstra et al., 2017), including the effects of flocculation (Horemans et al., 2020; Winterwerp, 2002). The width and bathymetry of the estuary are approximated by smooth profiles, focusing on the estuary-scale hydro- and SPM dynamics only. The model resolves the tidal and subtidal water motion and SPM concentration using a scaling and perturbation approach. This approach drastically reduces computation time, allowing us to carry out an extensive sensitivity analysis. Moreover, it simplifies the interpretation of the results as it allows us to study physical processes separately.

The water motion is forced at the mouth by a tidal signal and at the Upper Sea Scheldt boundary and two main tributaries by a constant water inflow that depends on the season. SPM dynamics are forced by a constant concentration of SPM at the mouth and an inflow of SPM at the Upper Sea Scheldt boundary, which is obtained from observations and equals the product of the subtidal SPM concentration and freshwater discharge. Although clearly detectable in the SPM observations at the dumping locations, we do not include dumping of dredge material because it acts locally on a much smaller time-scale (~hours) and does not show seasonality. Therefore, it is out of the scope of this study, which focuses on large-scale SPM dynamics on the seasonal scale. Moreover, we are interested in biotically affected, and not anthropogenically induced, erosion and flocculation. The longitudinal salinity profile is prescribed as a depth- and tide-independent sigmoid profile (Warner et al., 2005) that depends on the season (see Appendix B). This assumption is reasonable as the Scheldt is a well-mixed estuary in all seasons. Erosion of SPM is assumed to scale with the magnitude of the bed shear stress. The biotic impact on erosion is implicitly included in the corresponding

scaling factor called the erosion parameter M. This parameter is an intrinsic property of the sediment bed, including biotic effects, and determines the erosion flux E for a fixed bed shear stress τ_b and erodibility f:

$$E = M \left| \tau_b \right| f(a) \tag{1}$$

where a is the availability of easily erodible fine sediment and M is the erosion parameter.

The flocculation model describes the spatial and temporal evolution of the settling velocity of a single class of flocs. The effects of abiotic conditions (e.g., salinity, SPM concentration, and turbulence) are contained explicitly, whereas biotic effects (such as that of TEP) are implicitly included in the flocculation model. The parameter controlling the importance of biotic effects is denoted by λ, and is defined as the ratio of the minimal floc aggregation $k_A^{\min}$ and floc break-up parameter k_B. These two parameters characterize the flocculation properties given a fixed SPM concentration, salinity S, and shear rate G. For the model implementation of the shear rate G in summer and winter, we refer the reader to Appendix C. A careful scaling and perturbation analysis shows that λ impacts the settling velocity w_s (upto first order) (Horemans et al., 2020) as

$$w_s = \frac{1}{18} \frac{1}{\mu f_s} \frac{\rho_s - \rho_w}{\rho_s} \frac{g}{\sqrt{G}} \underbrace{\frac{k_A^{\min}}{k_B}}_{\lambda} f^{\text{sal}}(S) \cdot c + w_{s,\min}, \tag{2}$$

in which we assumed a fractal dimension $n_f = 2$ (see Appendix D for $n_f \neq 2$), spherical flocs, and that the floc Reynolds Number $\text{Re}_f = w_s D_f / \nu \ll 1$, where ν is the kinematic viscosity of water, and in which $w_{s,\min}$ is the settling velocity of the primary particles, μ is the dynamic viscosity of water, f_s is the shape factor of the flocs, ρ_s is the density of the primary particles, ρ_w is the density of water, g is the gravitational acceleration, c is the SPM concentration, and $f^{\text{sal}}(S)$ describes salinity driven flocculation by increasing the colloid stability for increasing salinity (Edzwald et al., 1974; Horemans et al., 2020). The impact of salinity driven flocculation is relatively low, which agrees with Einstein and Krone (1962), who showed that system-wide variations in salinity have only a minor influence on the bond strength. Salinity may also impact flocculation indirectly through, for example, its impact on TEP production (Alldredge et al., 1993; Bar-Zeev et al., 2015). This biotic impact is parametrically included in λ.

Reverse engineering model approach: To detect a biotically induced seasonality that impacts the seasonality in estuary-scale SPM dynamics, we follow P. H. Chen et al. (2018) by applying a reverse engineering model approach. This means that the biotically induced parameters λ and M are calibrated to observed SPM concentrations in summer and winter and that we statistically evaluate if the calibrated λ and M are the same in both seasons. We vary λ and M within a realistic range of values. The range in λ is 36–121×10^{-6} s$^{-1/2}$ m^2 and in M is 0.1–6×10^{-3} s m^{-1}, which is based on scaling (Horemans et al., 2020) and observations (Zhu et al., 2017), respectively.

As a first step in the reverse engineering approach, we average the SPM concentration observations of the various measuring campaigns at each depth. We assume that this averaged value approximates the residual SPM concentration similar to Dijkstra et al. (2019), Cox et al. (2019), and Horemans et al. (2020). This assumption is reasonable when the number of estimates is sufficiently large ($\gtrsim 10$), so by averaging the periodic temporal variability of the SPM concentration vanishes (Horemans et al., 2020). Here, we assume that the campaigns are homogeneously distributed within the spring-neap cycle and tidal phase, which was shown to be valid for the SPM sampling within the OMES framework between 1995 and 2015 (after 2015, the setup of the campaigns has not changed) (Vandenbruwaene et al., 2016). Moreover, we assume that each year between 2015 and 2018 corresponds to a similar SPM distribution on the estuary scale. To comply with the latter requirement, we leave out the year 2016 because of its exceptionally high amount of rainfall. Next, to compare the modeled residual SPM concentration to the time-averaged observed SPM concentration, we interpolate the time-averaged SPM observations to a grid with 16 cells in the along-channel direction (corresponding to the observation stations) and 50 cells in the vertical direction (independent of the water depth). The average SPM concentration in each cell is thus based on the average of 18 and 14 observations in summer and winter, respectively. In the remainder of this study, we do not consider the SPM concentration in the vertical cells closest to the sediment bed and water surface, as there are insufficient measurements there (due to distortions caused by air bubbles and high turbidity at the water surface and sediment bed, re-

spectively). As a second step, we quantify the accuracy of the modeled SPM concentration compared to the observations using a cost function that is based on a statistical two-tailed *t*-test. The cost function varies between 0 (perfect match between modeled SPM concentration and observations) and 1 (complete mismatch between modeled SPM concentration and observations). We refer the reader to Horemans et al. (2020) for a detailed description of the cost function. We exclude the SPM observations at the dumping locations (total of two stations) because here we expect high variability in SPM due to anthropogenic dumping of sediment, which is out of the scope of this study and not included in the model (see Section 2.3).

Finally, uncertainty in the SPM observations results in uncertainty in the optimal (cf. lowest cost function value) (λ, M) pairs. To quantify this uncertainty, we assume that the average SPM concentration in summer and winter is normally distributed with mean value equal to the mean of the OMES observations and standard deviation equal to the standard deviation in the OMES observations divided by the square root of the number of observations (i.e., 18 and 14 in summer and winter, respectively). To equate this to a probability distribution for the optimal (λ, M) pair, we randomly sample 500 averaged SPM concentrations from this normal distribution. Because the SPM concentrations in the vertical direction are not independent, we require that the relative deviation from the mean is equal at every depth at a given station, thus keeping the shape of the vertical time-averaged SPM profile fixed. Next, we calibrate λ and M for each sample. The resulting calibration is used to compute the standard deviation $\sigma_{\lambda,M}$ of the 500 (λ, M) pairs for summer and winter. Note we do not assume that λ and M are necessarily normally distributed. Finally, to quantitatively compare the optimal (λ, M) pairs in summer and winter conditions, we use this standard deviation $\sigma_{\lambda,M}$ to compute the difference of the optimal λ and M values in summer and winter conditions, relative to the corresponding standard deviation:

$$\Delta_\lambda = \frac{|\lambda^{\text{summer}} - \lambda^{\text{winter}}|}{\sqrt{(\sigma_\lambda^{\text{summer}})^2 + (\sigma_\lambda^{\text{winter}})^2}}, \qquad \Delta_M = \frac{|M^{\text{summer}} - M^{\text{winter}}|}{\sqrt{(\sigma_M^{\text{summer}})^2 + (\sigma_M^{\text{winter}})^2}}. \tag{3}$$

If $\Delta_{\lambda,M} < 1$, the average difference between summer and winter is less than one standard deviation and we will conclude that the difference of λ or M in winter and summer conditions is within the uncertainty of the SPM observations. The model parameter values for both the summer and winter conditions in the Scheldt estuary are given in Table 1. These values are either based on observations or calibration. Previous work indicated that the average summer discharge is representative, while the representative winter discharge is slightly above the average of 174 m^3 s^{-1} to correct for the large variability in discharges during winter (Horemans et al., 2020). The parameters corresponding to the depth- and tide-independent salinity profile (i.e., x_c and x_L) were fitted to salinity observations (see Appendix B). The system-averaged primary particle size D_p was estimated using observations (see Appendix E). If not mentioned explicitly, other parameter values used are presented in Horemans et al. (2020). For completeness, we repeated these parameter values in the supporting information attached to this study.

To test the robustness of the model, we apply a sensitivity analysis of two crucial parameters which are assumed to be fixed in the model: the primary particle size D_p and fractal dimension n_f. To apply a sensitivity analysis to the latter parameter, we have generalized the results presented in Horemans et al. (2020) for n_f $\neq 2$ (see Appendix D). Based on the experiments presented in Appendix E and the literature (Winterwerp & van Kesteren, 2004), we vary D_p and n_f between 4–25 μm and 1.7–3, respectively.

3. Results

In this section, we first show the seasonality of the in situ observations of SPM, floc size, Chl-a, and TEP concentrations in the Scheldt estuary. Next, we show the results of our model experiments, focusing on the seasonality in biotically affected calibration parameters λ and M and modeled SPM concentration. Finally, we present the sensitivity analysis of the modeled SPM concentration to D_p and n_f.

Table 1
Parameter List Used in Our Model Study in the Scheldt Estuary in Summer and Winter Conditions

	Variable	Definition	Value
Hydrodynamics	Q^{summer}	total river discharge in summer (calibrated)	40 m^3 s^{-1}
	Q^{winter}	total river discharge in winter (calibrated)	233 m^3 s^{-1}
Sediment	$c_{\text{upper Sea Scheldt}}$	subtidal SPM concentration at the Upper Sea Scheldt boundary (source)	0.035 kg m^{-3}
	M^{summer}	erosion parameter in summer (calibrated)	2.7×10^{-3} s m^{-1}
	M^{winter}	erosion parameter in winter (calibrated)	3.0×10^{-3} s m^{-1}
Turbulence	σ_ρ	Prandtl Schmidt number	0.5
	s_{f0}	bed roughness coefficient (calibrated)	4.22 mm s^{-1}
Flocculation	$k_A^{\text{min.}}$	nondimensional minimal aggregation coefficient	0.29
	f_s	shape factor	$\pi/6$
	n_f	fractal dimension of flocs	2
	D_p	diameter primary mud particles (source)	14×10^{-6} m
	ρ_s	density of SPM primary particles	2,650 kg m^{-3}
	ρ_w	reference density of water	1,000 kg m^{-3}
	λ^{summer}	ratio of minimal aggregation and floc break-up parameter in summer (calibrated)	72.5×10^{-6} s$^{-1/2}$ m^2
	λ^{winter}	ratio of minimal aggregation and floc break-up parameter in winter (calibrated)	65.9×10^{-6} s$^{-1/2}$ m^2
Salinity	s_{sea}	salinity boundary condition at the mouth	28.9 psu
	$x_c^{\text{sal, summer}}$	calibration parameter in postulated tanh salinity distribution in summer	51.9 km
	$x_L^{\text{sal, summer}}$	calibration parameter in postulated tanh salinity distribution in summer	31.2 km
	$x_c^{\text{sal, winter}}$	calibration parameter in postulated tanh salinity distribution in winter	38.3 km
	$x_L^{\text{sal, winter}}$	calibration parameter in postulated tanh salinity distribution in winter	24.8 km

3.1. Seasonality in the In Situ Observations

3.1.1. Seasonality in SPM

Figure 2 shows the observed time-averaged SPM concentration in summer and winter. Both in summer and winter, the concentrations range upto ~300 mg l^{-1} and typically increase with depth. In summer (see Figure 2a), two ETM are observed, located near 80 km (depicted by Ⓘ) and 120 km (depicted by ⒾⒾ). The ETM have a length of ~10 and 30 km, respectively. The ETM near 80 km is potentially due to anthropogenic dumping activities in this region (depicted by the vertical dashed lines), as mentioned above. In winter (see Figure 2b), the ETM at 80 km is also present, while the ETM near 120 km moves downstream, and shows significantly lower SPM concentrations (depicted by ⒾⒾ). Moreover, we detect an additional ETM near 60 km (depicted by ⒾⒾⒾ). We thus conclude that the SPM distribution in the Scheldt estuary shows strong seasonality, which complies with the results of Cox et al. (2019) and has been observed in many other estuaries (see Burchard et al., 2018 for a recent review).

3.1.2. Seasonality in Floc Size

Figure 3 shows the observed depth- and time-averaged floc size measured in summer and winter 2018. The error bars depict the standard error of the depth-averages corresponding to the various campaigns. In summer, we have an approximately constant depth-averaged floc size in the longitudinal direction. The floc sizes are in the order of 100 μm. In winter, the floc sizes decrease in the Upper Sea Scheldt beyond 120 km and are statistically smaller compared to the floc sizes in summer (one-tailed *t*-test, *p*-value $< 10^{-4}$). The averaged floc sizes in the Upper Sea Scheldt beyond 120 km are 115 and 77 μm in summer and winter, re-

(a) Observations of the SPM concentration (mg l^{-1}) in summer

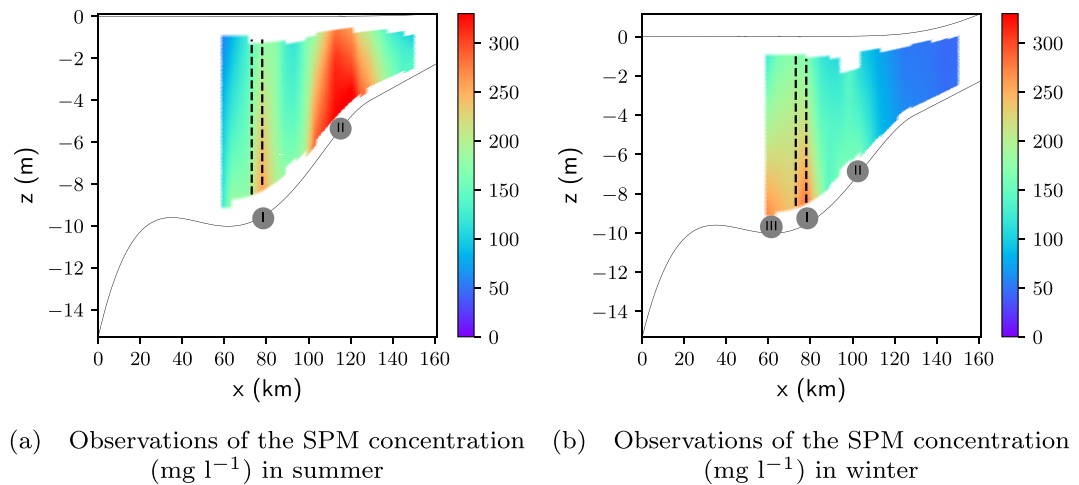(b) Observations of the SPM concentration (mg l^{-1}) in winter

Figure 2. Measured long-term time-averaged suspended particulate matter (SPM) concentration (mg l^{-1}) over the years 2015–2018 in (a) summer, showing two estuarine turbidity maxima (ETM) at locations (I) and (II), and (b) winter showing three ETM at locations (I), (II), and (III). The vertical dashed lines depict the dumping locations.

spectively. We thus conclude that, on the estuary scale (we observe a local anomaly near 60 km and 80 km), the floc sizes only show seasonality in the upstream part of the Scheldt estuary (>120 km). This is also valid using other averaging methods (see Appendix A).

3.1.3. Seasonality in Chl-a and TEP

The measured time-averages of the observations of Chl-a and TEP concentrations in summer and winter are shown in Figure 4. The error bars represent the standard error of the mean corresponding to the concentrations of the various campaigns. The Chl-a observations (see Figure 4a) show a strong seasonality in the Upper Sea Scheldt (>100 km), where the Chl-a concentration in summer is an order of magnitude larger than in winter. In contrast, although the TEP observations (see Figure 4b) show local seasonality at 58, 121, and 138 km, they do not show a significant system-wide seasonality in the Upper Sea Scheldt (one-tailed t-test, p-value > 0.38). The error bars corresponding to the TEP measurements are relatively large, especially in the Lower Sea Scheldt (<100 km). This is due to the relatively small number of estimates and the large temporal variability in TEP, a variability also observed in other estuarine and marine systems, such as the Neuse River Estuary (Wetz et al., 2009), the Pearl River estuary (Sun et al., 2012), and the Chesapeake bay (Malpezzi et al., 2013). What is most important within the scope of this study is that the Chl-a observations show seasonality whereas the TEP observations do not.
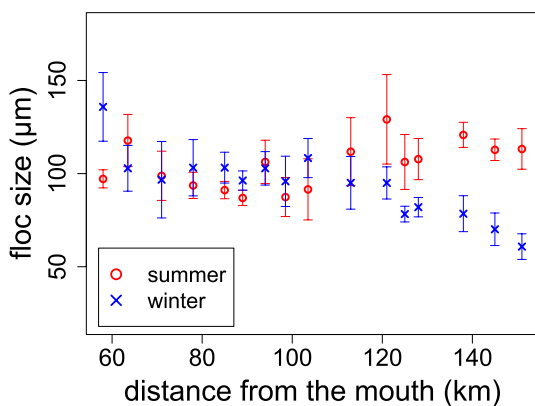
We conclude that we observe a clear seasonality in SPM and floc size dynamics beyond 120 km whereas some biotic properties show seasonality, and others do not; the contrast between the strong seasonality in Chl-a and the absence of seasonality in TEP on the estuary scale, both biotic factors reported to (indirectly) influence SPM dynamics, makes it difficult to use these observations as indicators for biotically induced seasonality in SPM. Therefore, the observations are complemented with model experiments which are shown in the following section.

3.2. Seasonality in the Model Experiments

3.2.1. Model Parameters λ and M

Minimizing the cost function separately for summer and winter results in an optimal parameter set $\lambda = 72.5 \times 10^{-6}$ s$^{-1/2}$ m^2, $M = 2.7 \times 10^{-3}$ s m^{-1} in summer (cost value equals 0.22) and $\lambda = 65.9 \times 10^{-6}$ s$^{-1/2}$ m^2,

Figure 3. Measured time- and depth-averaged floc size in summer (red) and winter (blue). The error bars depict the standard error of the estimates corresponding to the various campaigns.

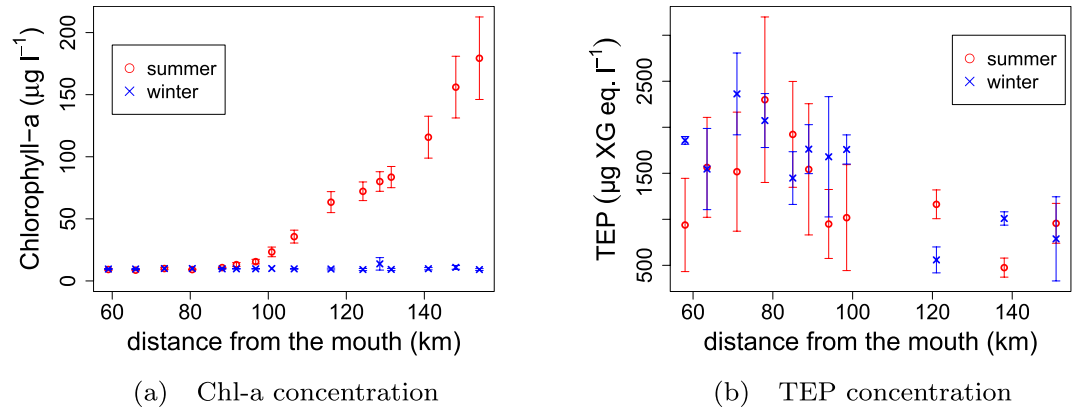(a)   Chl-a concentration

(b)   TEP concentration

Figure 4. (a) Measured time-averaged Chlorophyll-a (Chl-a) concentration in summer and winter over the years 2015–2018 and (b) corresponding measured transparent exopolymer particles (TEP) concentration of 2018. The error bars depict the standard error of the estimates corresponding to the various campaigns.

$M = 3.0 \times 10^{-3}$ s m^{-1} in winter (cost value equals 0.17). These optimal (λ, M) pairs thus show a weak ($\sim$10%) seasonality in both λ and M.

To explore the sensitivity of the model results to variations of the calibration parameters λ and M, Figure 5 shows the cost function as a function of λ (horizontal axis) and M (vertical axis), with the value of the cost function indicated by color. Optimal values are indicated by ①. The dark blue colors indicate the range of (λ, M) pairs with a good performance: the white dashed contours depict the cost function values which are 25% larger than the optimal cost function value. In summer (see Figure 5a), this contour covers a range with λ close to 70×10^{-6} s$^{-1/2}$ m^2 and $2 \times 10^{-3} < M < 5 \times 10^{-3}$ s m^{-1}. So, the optimal λ value is found in a relatively narrow parameter range and is quite insensitive to the value of M. In winter (see Figure 5b), the range of optimal values is around $\lambda \approx 60 \times 10^{-6}$ s$^{-1/2}$ m^2 and $M > 2 \times 10^{-3}$ s m^{-1}. Note our winter result slightly differs from the winter result presented in Horemans et al. (2020) because we added fluvial inflow of SPM at the Upper Sea Scheldt boundary (see Table 1), used a Prandtl Schmidt number of 0.5 instead of 1, and excluded the observations at the dumping locations in our calibration. We also included turbidity observations of 2018 in our calibration.
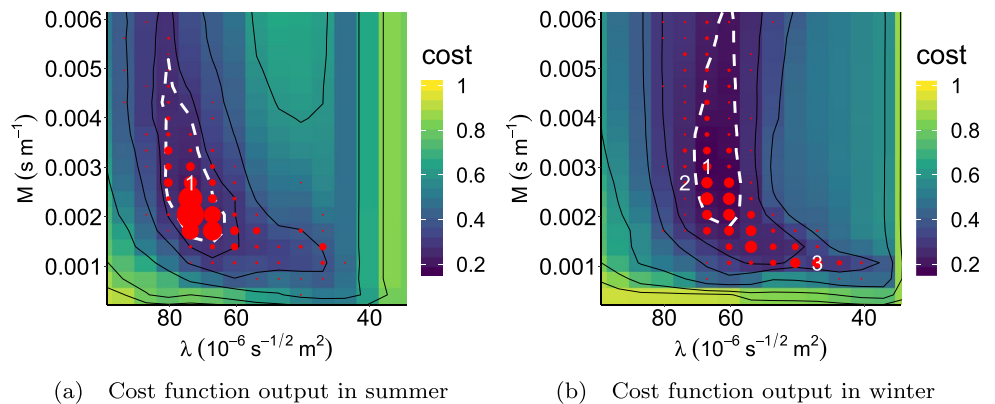

(a)   Cost function output in summer

(b)   Cost function output in winter

Figure 5. Cost function values for various λ and M calibrated to the observed residual SPM data set in (a) summer and (b) winter. The optimal calibration parameter set corresponds to ① $\lambda = 72.5 \times 10^{-6}$ s$^{-1/2}$ m^2, $M = 2.7 \times 10^{-3}$ s m^{-1} in summer and ① $\lambda = 65.9 \times 10^{-6}$ s$^{-1/2}$ m^2, $M = 3 \times 10^{-3}$ s m^{-1} in winter. The white dashed contours depict the cost function values which are 25% larger than the optimal cost function value. The red dots depict the probability density of the 500 (λ, M) pairs given the uncertainty in the residual SPM data set to which the model is calibrated. Bigger dots signify a higher probability density, while smaller dots signify a lower probability density. We choose two additional (λ, M) pairs, depicted by ② and ③, to study the impact of the choice in (λ, M) located in the zone of high probability density on the corresponding model output. The corresponding λ and M values are $\lambda = 72.5 \times 10^{-6}$ s$^{-1/2}$ m^2, $M = 2.7 \times 10^{-3}$ s m^{-1} (i.e., optimal summer conditions) and $\lambda = 45.3 \times 10^{-6}$ s$^{-1/2}$ m^2, $M = 1.1 \times 10^{-3}$ s m^{-1}, respectively.

The red dots in Figure 5 depict the probability density of (λ, M) given the uncertainty in the residual SPM data set to which the model is calibrated. Bigger dots signify a higher probability density, while smaller dots signify a lower probability density. We use these distributions of (λ, M) in summer and winter to quantitatively compare the optimal (λ, M) pairs using Equation 3 and detect a potential seasonality given the uncertainty in the residual SPM observations. The standard deviation of the λ and M distributions in the summer and winter conditions are $\sigma_\lambda^{\text{summer}} = 12.9 \times 10^{-6}$ s$^{-1/2}$ m^2, $\sigma_\lambda^{\text{winter}} = 10.5 \times 10^{-6}$ s$^{-1/2}$ m^2, $\sigma_M^{\text{summer}} = 0.9 \times 10^{-3}$ s m^{-1}, and $\sigma_M^{\text{winter}} = 1.4 \times 10^{-3}$ s m^{-1}. Consequently, the relative difference of the optimum values in summer and winter Δ (see Equation 3) for λ and M are $\Delta_\lambda = 0.4$ and $\Delta_M = 0.18$, respectively. We thus conclude that we do not detect seasonality in λ and M given the uncertainty of the residual SPM observations.

3.2.2. Seasonality in Modeled SPM Concentration

To further investigate the optimal calibration values of λ and M, we analyze the corresponding modeled SPM distribution for the optimal (λ, M) pair (see ① in Figure 5) for both summer and winter conditions. Given the estuary scale of the model and measurement uncertainty (cf. dark blue regions and distribution of (λ, M) pairs in Figure 5), we also show the SPM distribution corresponding to two additional (λ, M) pairs (see ② and ③ in Figure 5b). We require that these two pairs result in an acceptable model performance and are within the zone of high probability density in winter (red dots in Figure 5b). We choose the first pair to be equal to the optimal (λ, M) pair in summer and the second pair to be located in the second zone of (λ, M) pairs in winter where we detect a high probability density (depicted by the red dots in Figure 5b). The corresponding λ and M values are $\lambda = 72.5 \times 10^{-6}$ s$^{-1/2}$ m^2, $M = 2.7 \times 10^{-3}$ s m^{-1} and $\lambda = 45.3 \times 10^{-6}$ s$^{-1/2}$ m^2, $M = 1.1 \times 10^{-3}$ s m^{-1}, respectively. The corresponding cost function values equal 0.26 and 0.30, respectively.

Figure 6 shows the modeled SPM concentration in summer and winter using these values of λ and M and the corresponding observations. We present the model result and observations in summer in Figures 6a and 6b, respectively. Figure 6a shows two modeled ETM at the correct locations, that is, a weak ETM at the dumping location near 80 km and an ETM at 120 km (depicted by Ⓘ and ⒾⒾ, respectively). The length of the ETM covers ~10 and 30 km, respectively. Both model results and observations show concentrations upto ~300 mg l^{-1}. The model seems to overestimate the vertical gradient in SPM.

In winter, the model also captures the locations of the ETM for the optimal (λ, M) pair Ⓘ. The model result (see Figure 6c) and observations (see Figure 6d) both show an ETM near 80 km, ~10 km long (depicted by Ⓘ). The ETM in the model result potentially merged into the ETM caused by dumping activities, which are not considered in the model setup. The model also correctly captures the accumulation of SPM at 100 km (depicted by ②) and 60 km (depicted by ⒾⒾⒾ). The concentrations are in the order of 100–300 mg l^{-1}. What is most important within the scope of this paper is that the ETM near 120 km in summer shifts downstream to 100 km and an additional ETM near 60 km arises in winter. In other words, the model captures this seasonality in the ETM.

Figures 6e and 6f show the modeled SPM concentration corresponding to the two alternative (λ, M) pairs (see ② and ③ in Figure 5b). Compared to our previous result (see Figure 6c), no major change in case of parameter values associated with ② are observed (see Figure 6e). We observe a slight decrease in the SPM concentration, especially near the sediment bed, but the locations of the ETM are unchanged. The modeled SPM concentration corresponding to pair ③ (see Figure 6f) is different when compared to the optimal SPM concentration (see Figure 6c): the ETM near 60 km (depicted by ⒾⒾⒾ) vanished, the ETM near 80 and 100 km are still present (depicted by Ⓘ and ⒾⒾ, respectively). Although the cost function showed that is a reasonable calibration, visual inspection favors ① and ②. Acceptin ② gas a good fit further supports our conclusions that we can explain the observed seasonality in the estuary scale SPM distribution without requiring seasonality in biologically induced flocculation and erosion parameters. The seasonality in SPM can be captured by only accounting for seasonality in freshwater discharge and turbulence.

### 3.3. Sensitivity Analysis of the Modeled SPM Concentration to D_p and n_f

Figure 7 shows the sensitivity of the depth-averaged SPM concentration to D_p and n_f. The results of the SPM concentration in summer and winter are neither quantitatively nor qualitatively changed significantly when varying D_p (see Figures 7a and 7b) and n_f (see Figures 7c and 7d). To conclude, our sensitivity analysis
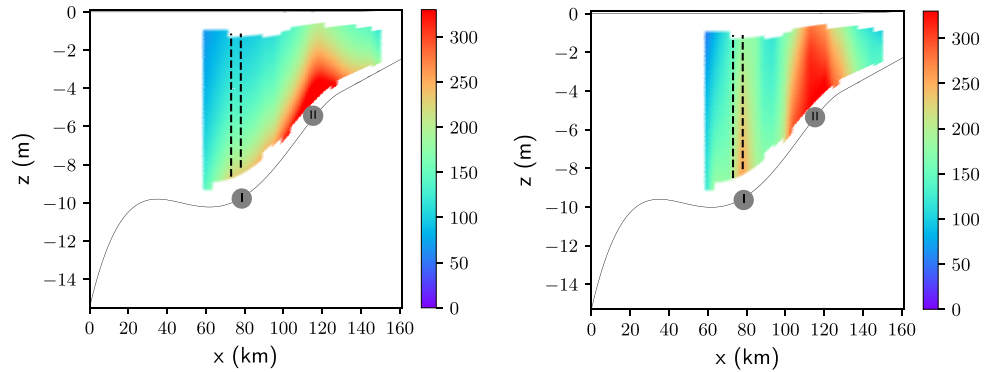
(a) Model output of the SPM concentration (mg l^{-1}) in summer ①

(b) Observations of the SPM concentration (mg l^{-1}) in summer
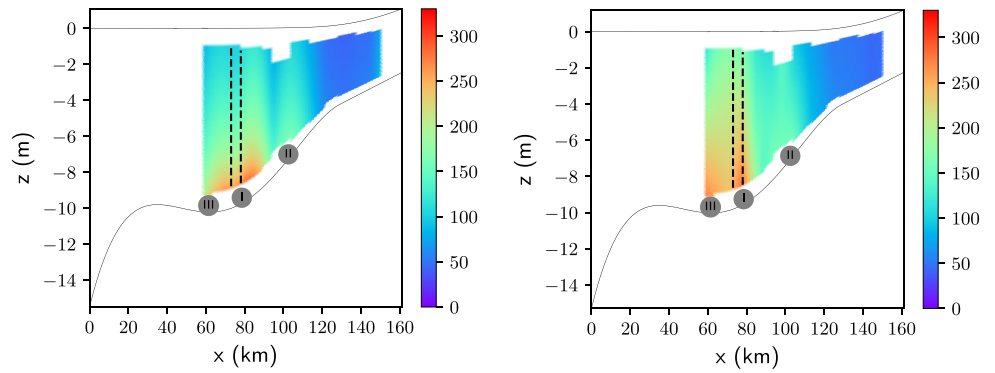
(c) Model output of the SPM concentration (mg l^{-1}) in winter ①

(d) Observations of the SPM concentration (mg l^{-1}) in winter
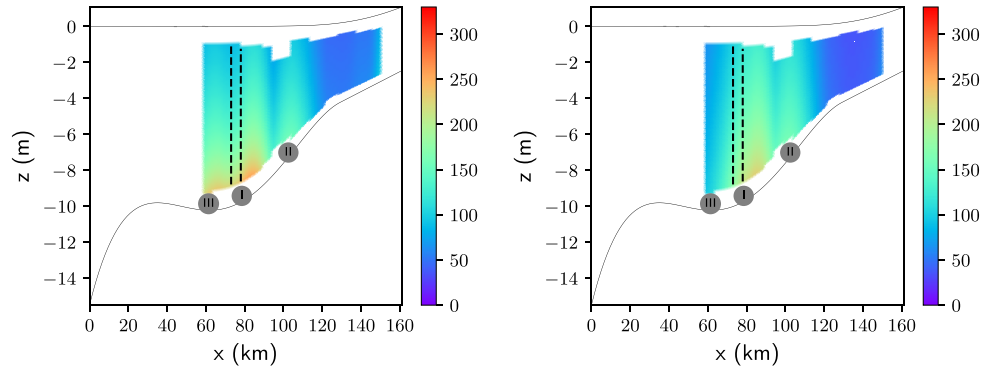
(e) Model output of the SPM concentration (mg l^{-1}) in winter ②

(f) Model output of the SPM concentration (mg l^{-1}) in winter ③

Figure 6. (a) Model output of the suspended particulate matter (SPM) concentration in summer. The optimal calibration parameters are ① $\lambda = 72.5 \times 10^{-6}$ s$^{-1/2}$ m^2 and $M = 3 \times 10^{-3}$ s m^{-1}. The vertical dashed lines depict the dumping locations, the symbols Ⓘ, ⒾⒾ, and ⓘⓘⓘ the locations of the observed estuarine turbidity maxima (ETM). (b) The long-term time-averaged SPM concentration observations (mg l^{-1}) in summer. (c) Model output of the SPM concentration in winter. The optimal calibration parameters are ① $\lambda = 65.9 \times 10^{-6}$ s$^{-1/2}$ m^2 and $M = 3.0 \times 10^{-3}$ s m^{-1}. (d) The long-term time-averaged SPM concentration observations (mg l^{-1}) in winter. (e–f) Model output of the SPM concentration in winter with ② $\lambda = 72.5 \times 10^{-6}$ s$^{-1/2}$ m^2, $M = 2.7 \times 10^{-3}$ s m^{-1} and ③ $\lambda = 45.3 \times 10^{-6}$ s$^{-1/2}$ m^2, $M = 1.1 \times 10^{-3}$ s m^{-1}, respectively.

(a) depth-averaged SPM concentration (in g l^{-1}) (b) depth-averaged SPM concentration (in g l^{-1})

(c) depth-averaged SPM concentration (in g l^{-1}) (d) depth-averaged SPM concentration (in g l^{-1})
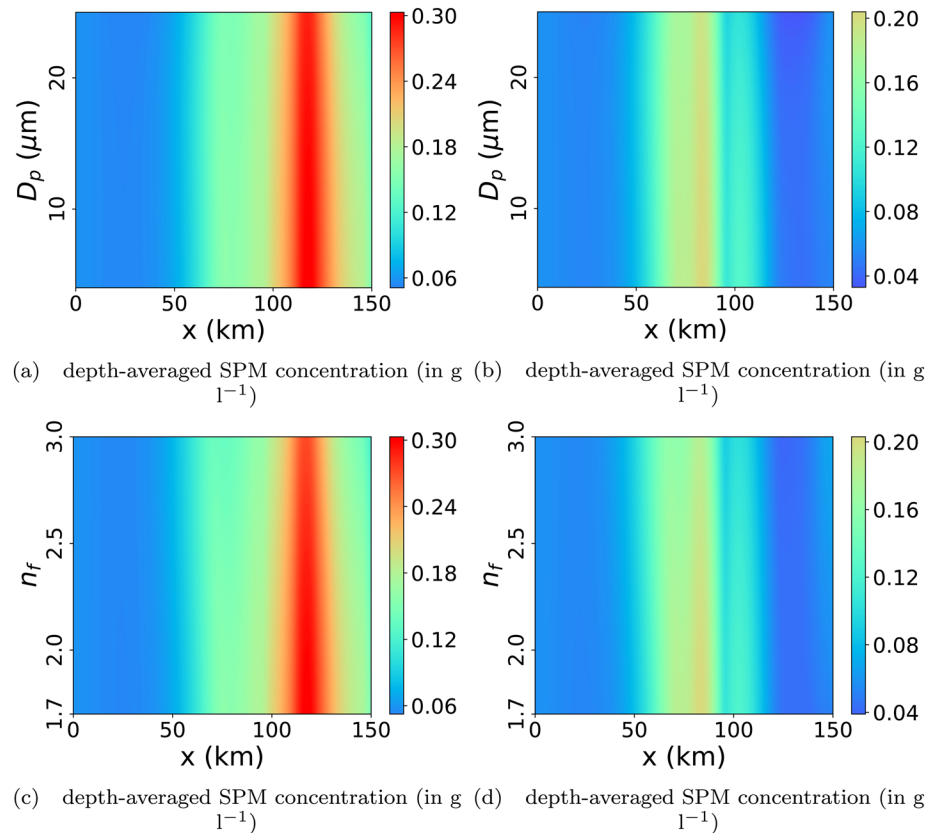
Figure 7. Sensitivity of the depth-averaged suspended particulate matter (SPM) concentration to the primary particle size D_p in (a) summer and (b) winter, and to the fractal dimension n_f in (c) summer and (d) winter.

of the modeled SPM concentration to D_p and n_f shows that our results and conclusions do not changes when choosing different parameter values.

4. Discussion

4.1. Model Performance and Reverse Engineering Approach

In this study, we aim to answer the question whether biotically induced seasonality has a dominant impact on the observed seasonality in SPM on the estuary scale in the Scheldt estuary. We take estuary scale to mean the location and approximate SPM concentration of the ETM, which are captured in our model. On this scale, seasonal differences in parameters representing biotic effects are not necessary. To be specific, any seasonal differences in optimal calibration of (λ, M) is within the uncertainty in the observations. Furthermore, choosing between optimally calibrated (λ, M) for summer and winter or equal (λ, M) in summer and winter only has an $\mathcal{O}(10^{-2})$ effect on the cost function representing goodness-of-fit. Moreover, by lumping all biotic effects of different nature and scale in only two parameters, our conclusions are only valid for the aggregated biotic effects on the large scale. This may still imply that the effect of individual biotic processes approximately cancels out against each other or are of significant importance locally, for example, in shallow areas.

4.2. Biotic Seasonality in Floc Size in the Scheldt Estuary

Various studies on the seasonality in floc size dynamics in the Scheldt estuary have been reported in the literature. These studies have linked these dynamics to the presence of biota but reading different conclusions. We explain the seasonality in floc size by seasonality in freshwater discharge and corresponding SPM

concentrations: a larger discharge results in flushing of the SPM concentrations and a larger shear rate locally at the upstream boundary (see Equation C1 and Figure C1). A decrease in SPM concentration and an increase in shear rate results in a decrease in floc size. Hence, it is worth discussing this.

Wartel and Francken (1998) measured in situ floc size between 40 and 100 km using a Benthos plankton camera, which measures in situ flocs ranging in size from 30 to 1,625 μm (the LISST 200x instrument we used measures floc sizes ranging from 1 to 500 μm). They found slightly lower averaged floc sizes of ∼70 μm, but did not measure a longitudinal trend in floc size between 60 and 100 km. Their averaged floc size of ∼90 μm at 110 km in winter and the absence of a significant seasonality (autumn vs. spring) of the floc size at 100 km compare well to our observations. They attributed this slightly larger floc size at 110 km to an increase in organic content and the presence of micro-organism, which excrete EPS (of which TEP is a subgroup).

In contrast, M. S. Chen et al. (2005) measured floc size locally at both a freshwater and brackish tidal flat in the Scheldt estuary. They used the so called "pipette-method" to determine floc sizes. Eisma et al. (1991) showed that observations using this method did not correlate to observations carried out using the in situ Benthos plankton camera. At the freshwater tidal flat (at ∼100 km), the mean floc size increased from ∼40 μm in winter upto 80 μm in spring. In the brackish tidal flat (at approximately 20 km), it increased from ∼30 μm in winter upto 90 μm in summer. Interestingly, the measured floc sizes in M. S. Chen et al. (2005) are significantly smaller in winter compared to our observations and the ones of Wartel and Francken (1998). M. S. Chen et al. (2005) also found a significant seasonality in floc size, which they linked to the presence of biota (i.e., organic content).

More recently, P. H. Chen et al. (2018) measured in situ floc sizes, again not in the estuary as a whole, but locally in the coastal region at the mouth (i.e., southern North Sea). By using a reverse engineering model approach, they found significant seasonality in floc strength, which was inversely related to floc break-up. More specifically, they showed that by decreasing the floc strength in winter (February and March) from $3 \ 10^{-11}$ N to $1 \ 10^{-11}$ N, their model simulations of floc size significantly improved when compared to the in situ observations. They attributed this seasonality in floc strength to biological effects (i.e., seasonality in TEP), which we did not observe in the Scheldt estuary as a whole (see Figure 4b). To conclude, floc size observations in the Scheldt estuary show different trends in the literature. These differences may be attributed to the usage of different methodologies (e.g., pipette method, in situ Benthos plankton camera) and the highly dependency on the system of interest (e.g., main channel, tidal flat, coastal region). Our observations comply with the main trends found by Wartel and Francken (1998), who also used an in situ method to measure floc size in the main channel.

5. Conclusions

In this study, we studied the importance of biotically induced seasonality in flocculation and erosion to seasonality in ETM formation applied to the Scheldt estuary. We presented in situ observations of SPM, floc size, Chl-a, and TEP. The SPM and floc size observations show seasonality. Chl-a and TEP observations show no correlation: Chl-a observations show a significant seasonality, whereas we do not detect seasonality in TEP on the estuary-scale. These unrelated results make it difficult to use observations of Chl-a and TEP alone as indicators for a potential seasonal impact of biota on the seasonality in ETM formation. Therefore, we combined the observations with a reverse engineering model approach to assess the aggregated impact of biotically induced seasonality in flocculation and erosion on the seasonality in large-scale ETM formation. In the model, this aggregated biotic impact through flocculation and erosion is implicitly parameterized by the ratio of the minimal floc aggregation and floc break-up parameter λ and the erosion parameter M.

Our model results suggest a weak (∼10%) seasonality in both λ and M, which is within the uncertainty of the SPM observations. Hence, to explain the observed seasonality in large-scale ETM formation, our results suggest that seasonality in λ and M is not required on the estuary scale. We capture the seasonality in SPM mainly by seasonality in freshwater discharge and resulting seasonality in SPM concentration and shear rate.

Appendix A: Floc Size Using Various Averaging Methods

To show that the estimated floc size is highly sensitive to the averaging method, we use two additional averaging methods: (1) the same averaging method as proposed by Sequoia Scientific (2019) but weighting the midpoint instead of the class number and (2) the median floc size by mass instead of volume. The difference between weighting by mass instead of volume depends on the structure of the flocs. Using our reference floc model assumption (fractal dimension is 2), averaging by mass is equivalent to averaging by area (Bowers et al., 2017). So, we divided the volume concentration of each size class by the corresponding midpoint.

Figure A1 shows the observed depth- and time-averaged floc size measured in summer and winter 2018 using the averaging method proposed by Sequoia Scientific (2019) (circles), weighting the midpoint instead of the size class number (triangles), and the time- and depth-averaged median floc size by mass (rectangles). The error bars depict the standard error of the depth averages corresponding to the various campaigns. Using other averaging methods may increase (weighting the midpoint by volume) or decrease (weighting by mass) the overall floc size. However, in all three averaging methods we observe seasonality in the upstream region of the Scheldt estuary. We thus conclude that, on the estuary scale (we observe a local anomaly near 60 and 80 km, depending on the averaging method), the floc sizes only show seasonality in the upstream part of the Scheldt estuary (>120 km).
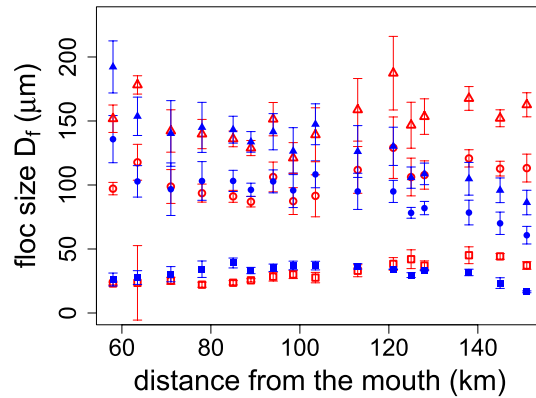

Figure A1. Measured time- and depth-averaged floc size in summer (red) and winter (blue) using the averaging method proposed by Sequoia Scientific (2019) (circles), weighting the midpoint instead of the size class number (triangles), and the time- and depth-averaged median floc size by mass (rectangles). The error bars depict the standard error of the estimates corresponding to the various campaigns.

Appendix B: Salinity Profile

Following Warner et al. (2005), we fit the salinity data measured in summer and winter in the Scheldt estuary to the following postulated salinity distribution:

$$\frac{s_{\text{sea}}}{2}\left(1 - \tanh\frac{x - x_c^{\text{Sal.}}}{x_L^{\text{Sal.}}}\right), \tag{B1}$$

with s_{sea} the salinity boundary condition at the mouth and $x_c^{\text{Sal.}}$ and $x_L^{\text{Sal.}}$ further undefined calibration parameters. Figure B1 shows the salinity data and corresponding data fit in summer and winter. Table 1 lists the corresponding parameter values.

Appendix C: Shear Rate in the Flocculation Model

Following Pejrup and Mikkelsen (2010), the shear rate G reads

$$G(x, \tilde{z}_1) = \sqrt{\frac{\langle u_* \rangle^3 (1 - \tilde{z}_1)}{\nu H \kappa' \tilde{z}_1}}, \tag{C1}$$
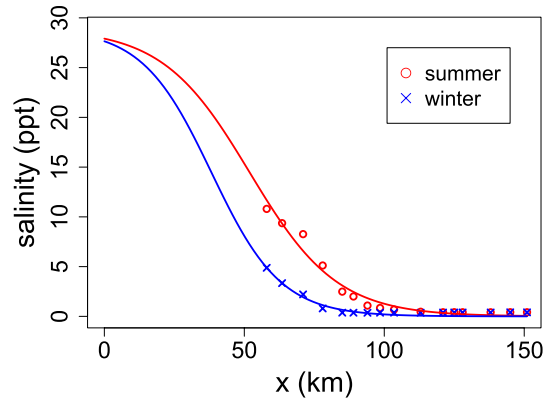
Figure B1. Measured salinity corresponding to our case study in the Scheldt estuary and corresponding data fit using Equation B1 in summer and winter.

in which x is the coordinate in the longitudinal direction, κ' is the Von Karman constant, ν is the kinematic viscosity of water, H is the water depth, $\tilde{z}_1 = z_1 / H$ is the relative water depth, and $\langle u_* \rangle$ is the subtidal friction velocity. To ensure that the model captures the impact of seasonality in river discharge on G, we define the subtidal friction velocity following Horemans et al. (2020) as

$$\langle u_* \rangle(x) = \frac{\kappa'}{\ln \dfrac{z_1(x)}{s_{f_0}}} \left\langle \left| u^0(x, z_1) + u_{\text{riv.}}(x, z_1) \right| \right\rangle, \tag{C2}$$

where z_1 is the distance in the logarithmic layer above the bed, s_{f_0} the bed roughness coefficient, u^0 the leading-order, longitudinal flow velocity, which consist of an M2 tidal signal (Chernetsky et al., 2010; Dijkstra et al., 2017), and $u_{\text{riv.}}$ the (subtidal) longitudinal, river-induced flow velocity. Consequently, an increase in freshwater discharge (cf. $u_{\text{riv.}}$) results in an increase in shear rate G. Following Horemans et al. (2020), we approximate G by its value at $z_1 = H/2$ and use this value $G(x, \tilde{z}_1 = 1 / 2)$ as a proxy for the whole water column, which is acceptable because vertical variations in G are relatively small in the logarithmic layer (typically $< 10\%$ in our case study). Moreover, we neglect tidal variation in G which is, within the scope of this paper, acceptable because the seasonality in tidal variability in our case study is small; the main difference in longitudinal water velocity between summer and winter is the riverine influence, locally at the upstream boundary, which is thus captured by the model. Figure C1 shows the shear rate in both summer and winter conditions.

The increase of freshwater discharge in winter increases the shear rate locally at the upstream boundary. Further downstream, between 100 and 140 km, it decreases the shear rate slightly because of a decrease of the tidal energy in this region.

Appendix D: Perturbation Approach for $n_f \neq 2$

We extend the flocculation model for general n_f. This requires a reanalysis of the results presented in Horemans et al. (2020). However, the same semi-analytical perturbation approach can be applied. At leading order $\mathcal{O}(1)$, a careful analysis shows that only the second term in the result of the leading order settling velocity w_s^0 presented in Horemans et al. (2020) changes:

$$w_s^0 = \beta c^0 + \frac{D_p}{\tilde{D}_f}(w_s^0)^{\frac{n_f - 2}{n_f - 1}}, \tag{D1}$$
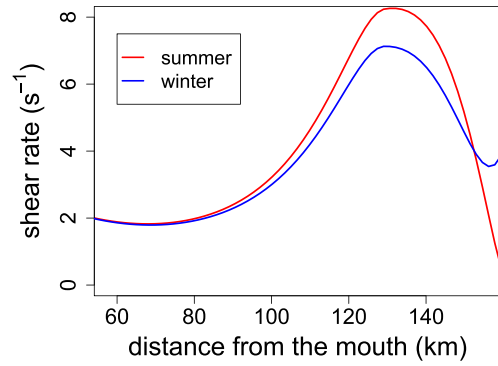
with

Figure C1. Modeled shear rate in summer and winter. The increase of freshwater discharge in winter increases the shear rate locally at the upstream boundary. Further downstream between 100 and 140 km, it decreases the shear rate slightly due to a decrease of tidal energy in this region.

$$\tilde{D}_f = 18^{\frac{1}{n_f-1}} \left(\frac{\mu D_p^{n_f-3}}{g(\rho_s - \rho_w)} \right)^{\frac{1}{n_f-1}},$$

(D2)

and where $\beta = (\rho_s - \rho_w)gk_A' / (18\,\mu f_s \rho_s \sqrt{G}k_B)$, with k_A' being the aggregation parameter, and c^0 is the leading order SPM concentration. For $n_f = 2$, the second term in Equation D1 is a constant value, being the settling velocity of the primary particles (Horemans et al., 2020). For $n_f \neq 2$, this second term is a function of both time and space. Consequently, at first order $\mathcal{O}(\epsilon)$ (with ϵ being the small perturbation parameter), the result becomes more complex but can still be easily solved to the first order settling velocity w_s^1:

$$w_s^1 = \frac{1}{-A\frac{(c^0)^2(3-2n_f)(w_s^0)^{-1+\frac{3-2n_f}{n_f-1}}}{n_f-1} + B\frac{c^0(2-n_f)(w_s^0)^{-1+\frac{2-n_f}{-1+n_f}}}{-1+n_f}} \times$$

$$\left\{ \frac{n_f}{n_f-1}K_v \left[2(w_s^0)^{\frac{1-2n_f}{n_f-1}}(\partial_z c^0)(\partial_z w_s^0) + c^0\frac{1-2n_f}{n_f-1}(w_s^0)^{\frac{2-3n_f}{n_f-1}}(\partial_z w_s^0)^2 \right] \right.$$

$$+(w_s^0)^{\frac{-n_f}{n_f-1}}(w_s^0\partial_z c^0 + c^0\partial_z w_s^0) - \frac{n_f}{n_f-1}c^0(w_s^0)^{\frac{1-2n_f}{n_f-1}}\left[\partial_t w_s^0 - K_v\partial_{zz}w_s^0 \right]$$

$$\left. -(w_s^0)^{\frac{-1}{n_f-1}}\partial_z c^0 + \frac{1}{n_f-1}c^0(w_s^0)^{\frac{-n_f}{n_f-1}}\partial_z w_s^0 + c_1\left[2\,Ac^0(w_s^0)^{\frac{3-2n_f}{n_f-1}} - B(w_s^0)^{\frac{2-n_f}{n_f-1}} \right] \right\},$$

(D3)

with

$$A = \frac{Gk_A'18^{\frac{3}{n_f-1}}\left(\frac{1}{D_p} \right)^{6-2n_f}\left(18^{\frac{1}{n_f-1}}\left(\frac{\mu D_p^{n_f-3}}{g(\rho_s - \rho_w)} \right)^{\frac{1}{n_f-1}} \right)^{-2n_f}\left(\frac{\mu D_p^{n_f-3}}{g(\rho_s - \rho_w)} \right)^{\frac{3}{n_f-1}}}{(fs\rho_s)^2},$$

(D4)

$$B = \frac{G^{1.5} k_B 18^{\frac{2}{n_f-1}} \left(\frac{1}{D_p}\right)^{3-n_f} \left(18^{\frac{1}{n_f-1}} \left(\frac{\mu D_p^{n_f-3}}{g(\rho_s - \rho_w)}\right)^{\frac{1}{n_f-1}}\right)^{-n_f} \left(\frac{\mu D_p^{n_f-3}}{g(\rho_s - \rho_w)}\right)^{\frac{2}{n_f-1}}}{f_s \rho_s}. \tag{D5}$$

Appendix E: Primary Particle Size and Density

Within the OMES campaign, we took 1 l samples from a bucket sample conducted at the water surface to estimate primary particle size (Maris et al., 2021). Samples were collected once a month at each station, which resulted in three samples per station for both summer and winter. At 58 km, we exceptionally have only two samples per season.

Primary particle size distribution was measured using a Mastersizer2000. The detection range of the Mastersizer2000 is 0.02–2,000 μm. After shaking the 1 l samples intensively, the samples were decanted in the dispersion unit of the Mastersizer2000 until the obscuration reached a value of $\sim$10%. We used the default absorption and refractive index (i.e., 0.1 and 1.52, respectively) and standard Lorenz-Mie method for spherical particles. The sampled were stirred and pumped with a frequency of 750 and 2,000 rpm, respectively, using tap water as a dispersant. Using this primary particle size distribution, we calculate the primary particle size corresponding to summer and winter using two averaging procedures. Figure E1 shows the primary particle size using a standard geometric average method often referred to as $D[1, 0]$. The corresponding system averaged value is 14.2 and 14.9 μm in summer and winter, respectively. The error bars represent the (Gaussian) standard error. Based on these estimates, we chose a primary particle size of 14 μm in our model.

The organic fractions of SPM, which have a density of $\sim$1,000 kg m^{-3}, can reach upto 30% in Scheldt estuary (Maris & Meire, 2017), and thus the organic fraction may have a relative impact via primary particle density (i.e., 2,650 kg m^{-3}) according to Fall et al. (2021) of

$$\Delta \rho_s = 1 - \frac{0.3 \cdot 1000 + 0.7 \cdot 2650}{2650} \sim 20\% \tag{E1}$$

This sensitivity was tested, and for such a decrease in ρ_s, we found a slight land-inward shift of the ETM in both summer and winter. We also observed this land-inward shift for decreasing λ (see Figure 6). This is to be expected because a decrease in ρ_s is equivalent to a decrease in λ, which follows from the factor $(\rho_s - \rho_w)/\rho_s$ in Equation 2.
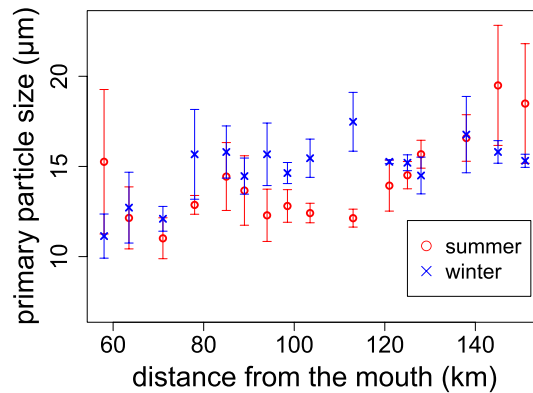

Figure E1. Primary particle size measured in summer and winter within the OMES (Dutch: "Onderzoek Milieu Effecten Sigmaplan") monitoring campaign.

Data Availability Statement

The turbidity, floc size, primary particle size, Chl-a, and TEP data set can be accessed through https://doi.org/10.14284/450, https://doi.org/10.14284/451, https://doi.org/10.14284/452, https://doi.org/10.14284/449, and https://doi.org/10.14284/453, respectively. The iFlow version 2.9 code with the flocculation extension and an input file example are available through https://doi.org/10.5281/zenodo.4560637.

References

Alldredge, A. L., Granata, T. C., Gotschalk, C. C., & Dickey, T. D. (1990). The physical strength of marine snow and its implications for particle disaggregation in the ocean. *Limnology and Oceanography*, 35, 1415–1428. https://doi.org/10.4319/lo.1990.35.7.1415

Alldredge, A. L., Passow, U., & Logan, B. E. (1993). The abundance and significance of a class of large, transparent organic particles in the ocean. *Deep Sea Research Part I: Oceanographic Research Papers*, 40, 1131–1140. https://doi.org/10.1016/0967-0637(93)90129-q

Allen, G. P., Salomon, J. C., Bassoullet, P., Du Penhoat, Y., & de Grandpré, C. (1980). Effects of tides on mixing and suspended sediment transport in macrotidal estuaries. *Sedimentary Geology*, 26, 69–90. https://doi.org/10.1016/0037-0738(80)90006-8

Bar-Zeev, E., Passow, U., Romero-Vargas Castrillón, S., & Elimelech, M. (2015). Transparent exopolymer particles: From aquatic environments and engineered systems to membrane biofouling. *Environmental Science and Technology*, 49, 691–707. https://doi.org/10.1021/es5041738

Bowers, D. G., McKee, D., Jago, C. F., & Nimmo-Smith, W. A. M. (2017). The area-to-mass ratio and fractal dimension of marine flocs. *Estuarine, Coastal and Shelf Science*, 189, 224–234. https://doi.org/10.1016/j.ecss.2017.03.026

Brouwer, R. L., Schramkowski, G. P., Dijkstra, Y. M., & Schuttelaars, H. M. (2018). Time evolution of estuarine turbidity maxima in well-mixed, tidally dominated estuaries: The role of availability- and erosion-limited conditions. *Journal of Physical Oceanography*, 48, 1629–1650. https://doi.org/10.1175/jpo-d-17-0183.1

Burchard, H., Schuttelaars, H. M., & Ralston, D. K. (2018). Sediment trapping in estuaries. *Annual Review of Marine Science*, 10, 371–395. https://doi.org/10.1146/annurev-marine-010816-060535

Chen, M. S., Wartel, S., & Temmerman, S. (2005). Seasonal variation of floc characteristics on tidal flats, the Scheldt estuary. *Hydrobiologia*, 540, 181–195. https://doi.org/10.1007/s10750-004-7143-6, http://link.springer.com/10.1007/s10750-004-7143-6

Chen, P. H., Yu, J. C. S., & Fettweis, M. (2018). Modeling storm-influenced suspended particulate matter flocculation using a tide-wave-combined biomineral model. *Water Environment Research*, 90, 244–257. https://doi.org/10.2175/106143017x15131012152799

Chernetsky, A. S., Schuttelaars, H. M., & Talke, S. A. (2010). The effect of tidal asymmetry and temporal settling lag on sediment trapping in tidal estuaries. *Ocean Dynamics*, 60, 1219–1241. https://doi.org/10.1007/s10236-010-0329-8

Claquin, P., Probert, I., Lefebvre, S., & Veron, B. (2008). Effects of temperature on photosynthetic parameters and TEP production in eight species of marine microalgae. *Aquatic Microbial Ecology*, 51, 1–11. https://doi.org/10.3354/ame01187

Cox, T. J. S., Maris, T., Van Engeland, T., Soetaert, K., & Meire, P. (2019). Critical transitions in suspended sediment dynamics in a temperate meso-tidal estuary. *Scientific Reports*, 9, 12745. https://doi.org/10.1038/s41598-019-48978-5

Dijkstra, Y. M., Brouwer, R. L., Schuttelaars, H. M., & Schramkowski, G. P. (2017). The iFlow modelling framework v2.4: A modular idealized process-based model for flow and transport in estuaries. *Geoscientific Model Development*, 10, 2691–2713. https://doi.org/10.5194/gmd-10-2691-2017

Dijkstra, Y. M., Schuttelaars, H. M., & Schramkowski, G. P. (2019). Can the Scheldt River Estuary become hyperturbid? *Ocean Dynamics*, 69, 809–827. https://doi.org/10.1007/s10236-019-01277-z

Dyer, K. R. (1989). Sediment processes in estuaries: Future research requirements. *Journal of Geophysical Research*, 94, 14327–14339. https://doi.org/10.1029/jc094ic10p14327

E. W. Rice, R. B. Baird, & A. D. Eaton (Eds.), (2017). *Standard methods for the examination of water and wastewater* (23rd ed.). American Public Health Association, American Water Works Association, and Water Environment Federation.

Edzwald, J. K., Upchurch, J. B., & O'Melia, C. R. (1974). Coagulation in estuaries. *Environmental Science and Technology*, 8, 58–63. https://doi.org/10.1021/es60086a003

Einstein, H. A., & Krone, R. B. (1962). Experiments to determine modes of cohesive sediment transport in salt water. *Journal of Geophysical Research*, 67, 1451–1461. https://doi.org/10.1029/jz067i004p01451

Eisma, D., Bernard, P., Cadée, G. C., Ittekkot, V., Kalf, J., Laane, R., et al. (1991). Suspended-matter particle size in some West-European estuaries; part I: Particle-size distribution. *Netherlands Journal of Sea Research*, 28(3), 193–214. https://doi.org/10.1016/0077-7579(91)90017-U

Fall, K. A., Friedrichs, C. T., Massey, G. M., Bowers, D. G., & Smith, S. J. (2021). The importance of organic content to fractal floc properties in estuarine surface waters: Insights from video, LISST, and pump sampling. *Journal of Geophysical Research: Oceans*, 126, e2020JC016787. https://doi.org/10.1029/2020JC016787

Fettweis, M., Baeye, M., Van der Zande, D., Van den Eynde, D., & Joon Lee, B. (2014). Seasonality of floc strength in the southern North Sea. *Journal of Geophysical Research: Oceans*, 119, 1911–1926. https://doi.org/10.1002/2013jc009750

Frostick, L. E., & McCave, I. N. (1979). Seasonal shifts of sediment within an estuary mediated by algal growth. *Estuarine and Coastal Marine Science*, 9, 569–576. https://doi.org/10.1016/0302-3524(79)90080-x

Horemans, D. M. L., Dijkstra, Y. M., Schuttelaars, H. M., Meire, P., & Cox, T. J. S. (2020). Unraveling the essential effects of flocculation on large-scale sediment transport patterns in a tide-dominated estuary. *Journal of Physical Oceanography*, 50, 1957–1981. https://doi.org/10.1175/jpo-d-19-0232.1

IMDC. (2016). *Monitoringprogramma Flexibel Storten. Multivariate analyse van metingen van sedimentconcentratie in de Zeeschelde* (WL Reports No. I/RA/11353/15.228/THL). Antwerpen, Belgium: IMDC.

Kandiah, A. (1974). *Fundamental aspects of surface erosion of cohesive soils* (Doctoral dissertation). Davis, CA: University of California. Retrieved from https://books.google.be/books?id=AdqrnQEACAAJ

Kappenberg, J., & Grabemann, I. (2001). Variability of the mixing zones and estuarine turbidity maxima in the Elbe and Weser estuaries. *Estuaries*, 24, 699–706. https://doi.org/10.2307/1352878

Kranenburg, C. (1994). The fractal structure of cohesive sediment aggregates. *Estuarine, Coastal and Shelf Science*, 39, 451–460. https://doi.org/10.1006/ecss.1994.1075

Lai, H., Fang, H., Huang, L., He, G., & Reible, D. (2018). A review on sediment bioflocculation: Dynamics, influencing factors and modeling. *The Science of the Total Environment*, *642*, 1184–1200. https://doi.org/10.1016/j.scitotenv.2018.06.101

MacCready, P., & Geyer, W. R. (2010). Advances in estuarine physics. *Annual Review of Marine Science*, *2*, 35–58. https://doi.org/10.1146/annurev-marine-120308-081015

Malarkey, J., Baas, J. H., Hope, J. A., Aspden, R. J., Parsons, D. R., Peakall, J., et al. (2015). The pervasive role of biological cohesion in bedform development. *Nature Communications*, *6*, 1–6. https://doi.org/10.1038/ncomms7257

Malpezzi, M. A., Sanford, L. P., & Crump, B. (2013). Abundance and distribution of transparent exopolymer particles in the estuarine turbidity maximum of Chesapeake Bay. *Marine Ecology Progress Series*, *486*, 23–35. https://doi.org/10.3354/meps10362

Maris, T., Claus, J., & Meire, P. (2021a). *Floc size distribution measured monthly or bi-weekly in the Zeeschelde at 12 stations using a LISST 200x instrument*. (Data set. Ecosystem Management Research Group - Uantwerpen; International Marine and Dredging Consultants nv.; De Vlaamse Waterweg; Belgium). https://doi.org/10.14284/451

Maris, T., Claus, J., & Meire, P. (2021b). *Turbidity and suspended sediment concentration profiles measured monthly or bi-weekly in the Zeeschelde at 16 stations using an obs instrument*. (Data set. Ecosystem Management Research Group - Uantwerpen; International Marine and Dredging Consultants nv.; De Vlaamse Waterweg; Belgium). https://doi.org/10.14284/450

Maris, T., & Meire, P. (2017). *Omes rapport 2016. Onderzoek naar de gevolgen van het Sigmaplan, baggeractiviteiten en havenuitbreiding in de Zeeschelde op het milieu (Tech. Rep. Nos. Report Ecosystem Management Research Group ECOBE, 017-R206)*. Antwerp, Belgium: University of Antwerp. Retrieved from www.vliz.be/imisdocs/publications/310259.pdf

Maris, T., & Meire, P. (2021). *Chlorophyll a measured monthly or bi-weekly in the Zeeschelde at 16 stations*. (Data set. Ecosystem Management Research Group - Uantwerpen; De Vlaamse Waterweg; Belgium). https://doi.org/10.14284/449

Maris, T., Van Der Spiet, T., & Meire, P. (2021). *Primary particle size distribution measured monthly in the Zeeschelde at 16 stations using a mastersizer2000 instrument*. (Data set. Ecosystem Management Research Group - Uantwerpen; De Vlaamse Waterweg; Belgium). https://doi.org/10.14284/452

Meire, P., Ysebaert, T., Damme, S. V., Bergh, E. V. d., Maris, T., & Struyf, E. (2005). The Scheldt estuary: A description of a changing ecosystem. *Hydrobiologia*, *540*, 1–11. https://doi.org/10.1007/s10750-005-0896-8

Mietta, F., Chassagne, C., Manning, A. J., & Winterwerp, J. C. (2009). Influence of shear rate, organic matter content, pH and salinity on mud flocculation. *Ocean Dynamics*, *59*, 751–763. https://doi.org/10.1007/s10236-009-0231-4

Partheniades, E. (1965). Erosion and deposition of cohesive soils. *Journal of the Hydraulics Division*, *91*, 105–139. https://doi.org/10.1061/jyceaj.0001165

Passow, U. (2002). Transparent exopolymer particles (TEP) in aquatic environments. *Progress in Oceanography*, *55*(3–4), 287–333. https://doi.org/10.1016/s0079-6611(02)00138-6

Passow, U., & Alldredge, A. L. (1995). A dye-binding assay for the spectrophotometric measurement of transparent exopolymer particles (TEP). *Limnology and Oceanography*, *40*, 1326–1335. https://doi.org/10.4319/lo.1995.40.7.1326

Passow, U., Shipe, R. F., Murray, A., Pak, D. K., Brzezinski, M. A., & Alldredge, A. L. (2001). The origin of transparent exopolymer particles (TEP) and their role in the sedimentation of particulate matter. *Continental Shelf Research*, *21*, 327–346. https://doi.org/10.1016/S0278-4343(00)00101-1

Paterson, D. M., & Black, K. S. (1999). Water flow, sediment dynamics and benthic biology. *Advances in Ecological Research*, *29*, 155–193. https://doi.org/10.1016/S0065-2504(08)60193-2

Pejrup, M., & Mikkelsen, O. A. (2010). Factors controlling the field settling velocity of cohesive sediment in estuaries. *Estuarine, Coastal and Shelf Science*, *87*, 177–185. https://doi.org/10.1016/j.ecss.2009.09.028

Plancke, Y., Van De Moortel, I., Hertogs, R., Vereecken, H., Vos, G., Verdoodt, N., et al. (2017). *Monitoring Effecten Ontwikkelingsschets (MONEOS) - Jaarboek monitoring 2016: Deelrapport 6 - Factual data rapportage van monitoring waterbeweging en fysische parameters in de Zeeschelde in 2016 (WL Reports No. 12_070_6)*. Antwerpen: Flanders Hydraulics Research. Retrieved from https://publicaties.vlaanderen.be/download-file/26407

Ralston, D. K., Geyer, W. R., & Warner, J. C. (2012). Bathymetric controls on sediment transport in the Hudson River estuary: Lateral asymmetry and frontal trapping. *Journal of Geophysical Research*, *117*, C10013. https://doi.org/10.1029/2012jc008124

Sequoia Scientific. (2019). *How to compute the mean particle diameter from a LISST volume distribution*. Sequoia Scientific. Retrieved from http://www.sequoiasci.com/article/how-to-compute-the-mean-particle-diameter-from-a-lisst-volume-distribution-2/

Stal, L. J. (2010). Microphytobenthos as a biogeomorphological force in intertidal sediment stabilization. *Ecological Engineering*, *36*, 236–245. https://doi.org/10.1016/j.ecoleng.2008.12.032

Stanford, L. P., Suttles, S. E., & Halka, J. P. (2001). Reconsidering the physics of the Chesapeake Bay estuarine turbidity maximum. *Estuaries*, *24*, 655–669. https://doi.org/10.2307/1352874

Sun, C.-C., Wang, Y.-S., Li, Q. P., Yue, W.-Z., Wang, Y.-T., Sun, F.-L., & Peng, Y.-L. (2012). Distribution characteristics of transparent exopolymer particles in the Pearl River estuary, China. *Journal of Geophysical Research*, *117*. https://doi.org/10.1029/2012JG001951

Uncles, R. J., Stephens, J. A., & Harris, C. (2006). Runoff and tidal influences on the estuarine turbidity maximum of a highly turbid system: The upper Humber and Ouse Estuary, UK. *Marine Geology*, *235*, 213–228. https://doi.org/10.1016/j.margeo.2006.10.015

Vandenbruwaene, W., Vanlede, J., Plancke, Y., Verwaest, T., & Mostaert, F. (2016). *Slibbalans zeeschelde: Deelrapport 4. Historische evolutie SPM (WL Reports No. 00_029_8)*. Antwerp, Belgium: Waterbouwkundig Laboratorium/Antea Group. Retrieved from http://www.vliz.be/imisdocs/publications/ocrd/304069.pdf

van Leussen, W. (1994). *Estuarine macroflocs and their role in fine-grained sediment transport* (Doctoral dissertation). Utrecht University. Retrieved from http://publicaties.minienm.nl/documenten/estuarine-macroflocs-and-their-role-in-fine-grained-sediment-tra

Verney, R., Lafite, R., & Brun-Cottan, J.-C. (2009). Flocculation potential of estuarine particles: The importance of environmental factors and of the spatial and seasonal variability of suspended particulate matter. *Estuaries and Coasts*, *32*, 678–693. https://doi.org/10.1007/s12237-009-9160-1

Vyverman, W., Maris, T., Daveloose, I., Sabbe, K., & Meire, P. (2021). *Transparent exopolymer particles measured monthly in the zeeschelde at 11 stations*. (Data set. Protistology & Aquatic Ecology - Ugent; Ecosystem Management Research Group - Uantwerpen; De Vlaamse Waterweg, Belgium). https://doi.org/10.14284/453

Warner, J. C., Geyer, W. R., & Lerczak, J. A. (2005). Numerical modeling of an estuary: A comprehensive skill assessment. *Journal of Geophysical Research*, *110*, 1–13. https://doi.org/10.1029/2004JC002691

Wartel, S., & Francken, F. (1998). *Sedimenttransport en sedimentatieprocessen in de Schelde tussen zandvliet en gent: Suspensiemateriaal in de Schelde. Tech. Rep. No. AMIS DS6.1-7-vol. III*. Brussels, Belgium: Royal Belgian Institute of Natural Sciences. Retrieved from www.vliz.be/imisdocs/publications/ocrd/224340.pdf

Waterinfo.be. (2019). *Measurements and predictions of Waterinfo.be [data]. De Vlaamse Milieumaatschappij and Waterbouwkundig Laboratorium and Maritieme Dienstverlening en Kust and De Vlaamse Waterweg NV*. Retrieved from https://www.waterinfo.be/

Wetz, M. S., Robbins, M. C., & Paerl, H. W. (2009). Transparent exopolymer particles (TEP) in a river-dominated estuary: Spatial-temporal distributions and an assessment of controls upon TEP formation. *Estuaries and Coasts*, *32*, 447–455. https://doi.org/10.1007/s12237-009-9143-2

Winterwerp, J. C. (2002). On the flocculation and settling velocity of estuarine mud. *Continental Shelf Research*, *22*(9), 1339–1360. https://doi.org/10.1016/s0278-4343(02)00010-9

Winterwerp, J. C., & van Kesteren, W. G. M. (2004). *Introduction to the physics of cohesive sediment in the marine environment*. Amsterdam, the Netherlands: Elsevier Science.

Zhu, Q., Wang, Z., Yang, S. L., & van Prooijen, B. (2017). *Sediment dynamics on intertidal mudflats: A study based on in situ measurements and numerical modelling*. Delft: Doctoral dissertation, Delft University of Technology. https://doi.org/10.4233/UUID:5F094E4B-FEF9-4216-ABBE-3277ADC90B28